Supporting information

Anion-controlled Zn(II) Coordination Polymers with 1-(tetrazo-5-yl)-3-(triazo-1-yl) benzene as an Assembling Ligand: Synthesis, Characterization, and Efficient Detection of Tryptophan in Water

Han-Xu Sun,[†] *Jie Zhou,**[,†] *Zhen Zhang,*[†] *Mei He,*[†] *Lian-Cheng He,*[†] *Lin Du,*[†] *Ming-Jin Xie,*[†] *and Qi-Hua Zhao**[,†]

[†]Key Laboratory of Medicinal Chemistry for Natural Resource, Ministry of Education; Yunnan Research & Development Center for Natural Products; School of Chemical Science and Technology, Yunnan University, Kunming, 650091, P. R. China

Content

(5) Figure S4. π···π interaction in **2**.

(6) Figure S5. Schematic representation indicating the dihedral angles between the benzene ring and tetrazole/triazole rings.

(7) Figure S6. TGA curves of **1** and **2**.

(8) Figure S7. Water stability of **1** and **2**.

(9) Figure S8. The pH stability of **1** and **2**.

(10) Figure S9. The UV-Vis of the ligand and by TD-DFT calculated.

(11) Figure S10. Solid-state fluorescence of **1**, **2** and Httb ligand.

(12) Figure S11. The PXRD pattern of **1** and **2** circulating five times.

(13) Figure S12. Recovery rate of **1** and **2**.

(14) Figure S13. Cytotoxicity test of **2**.

(15) Figure S14. Variable temperature fluorescence of **2**.

(16) Figure S15. The PXRD pattern of **1** and **2** in tryptophan aqueous.

(17) Figure S16. Nonlinear quenching plot of **1** and **2** with increasing tryptophan concentration.

(18) Figure S17. excitation wavelength and emission wavelength of **1** and **2** and tryptophan UV-Vis absorption spectrum.

(19) Figure S18. Fluorescence lifetime of **1** and **2**.

(20) Figure S19. Two-dimensional fingerprint peak of **1**.

(21) Figure S20. Two-dimensional fingerprint peak of **2**.

(22) Figure S21. The relative contribution of the contacts between the various molecules and nitrogen atoms.

(23) Figure S22. Hirshfeld surface mapped with d_{norm} of **1**.

(24) Figure S23. Hirshfeld surface mapped with d_{norm} of **2**.

(25) Figure S24. The PXRD patterns of **1** and **2**.

(26). **Figure S25.** SEM of **1** and **2**.

(27) Figure S26. The IR of **1**, **2**, and Httb

(28) Figure S27. Liquid Fluorescence of Ligand and the fluorescence curve after adding tryptophan.

(29) Figure S28. Raman spectra of **1**, **2** and after adding tryptophan respectively.

(30) Table S1. Crystallographic data for **1** and **2**.

(31) Table S2. the selected bond distance and angle for **1**.

(32) Table S3. the selected bond distance and angle for **2**.

(33) Table S4. Hydrogen bonds for **1**.

(34) Table S5. Hydrogen bonds for **2**.

(35) Table S6. Calculate the S1 electron transfer energy of the ligand and the contribution rate of each orbital.

(36) Table S7. Calculation results of singlet state energy level and the corresponding wavelength of excitation light of Httb and selected amino acids.

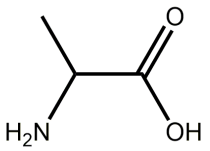

Alanine (Ala)

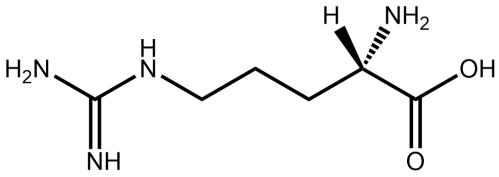

Arginine (Arg)

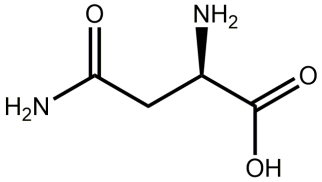

Asparagine (Asn)

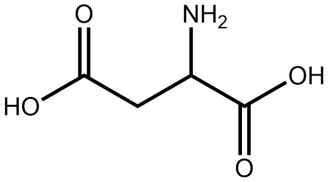

Asparticacid (Asp)

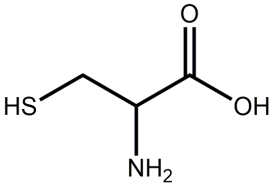

Cysteine (Cys)

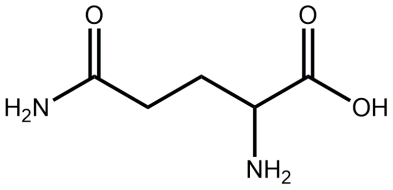

Glutamine (Gln)

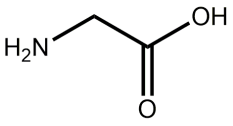

Glycine (Gly)

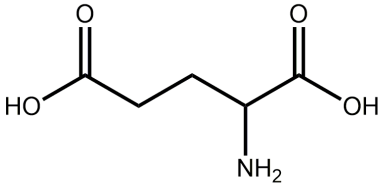

Glutamicacid (Glu)

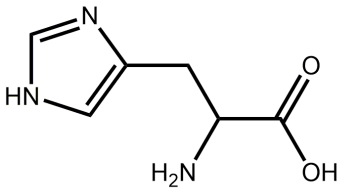

Histidine (His)

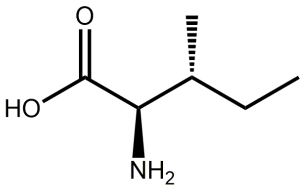

Isoleucine (Ile)

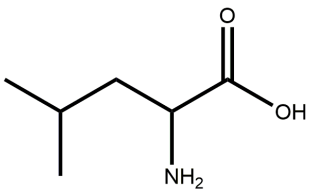

Leucine (Leu)

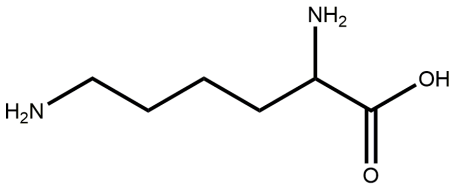

Lysine (Lys)

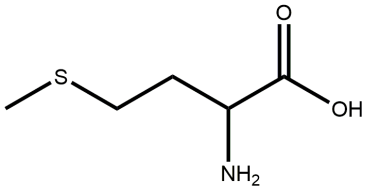

Methionine (Met)

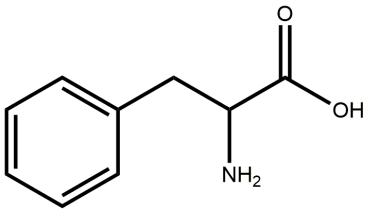

Phenylalanine (Phe)

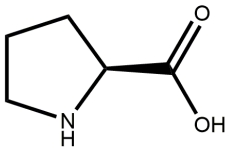

Proline (Pro)

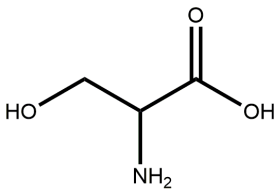

Serine (Ser)

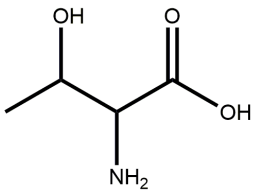

Threonine (Thr)

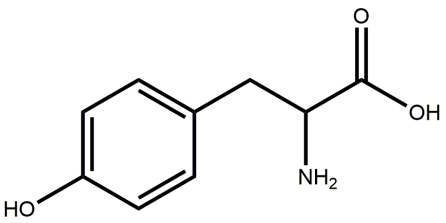

Tyrosine (Tyr)

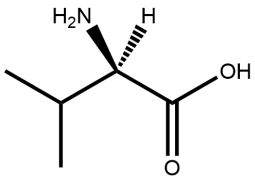

Valine (Val)

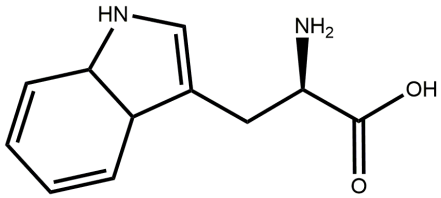

Tryptophan (Trp)

Scheme S1. 20 common amino acid structures and abbreviations.

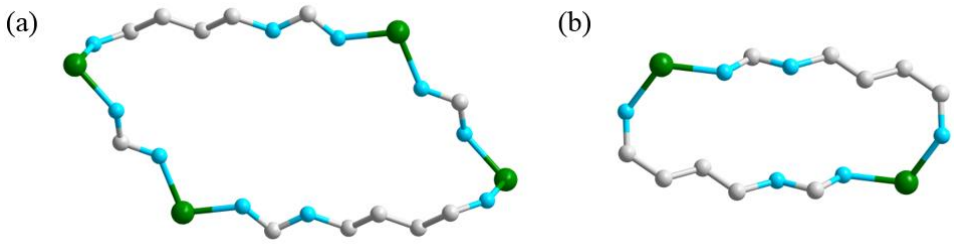

Figure S1. Schematic representation of the 26- and 18-member rings in **1**.

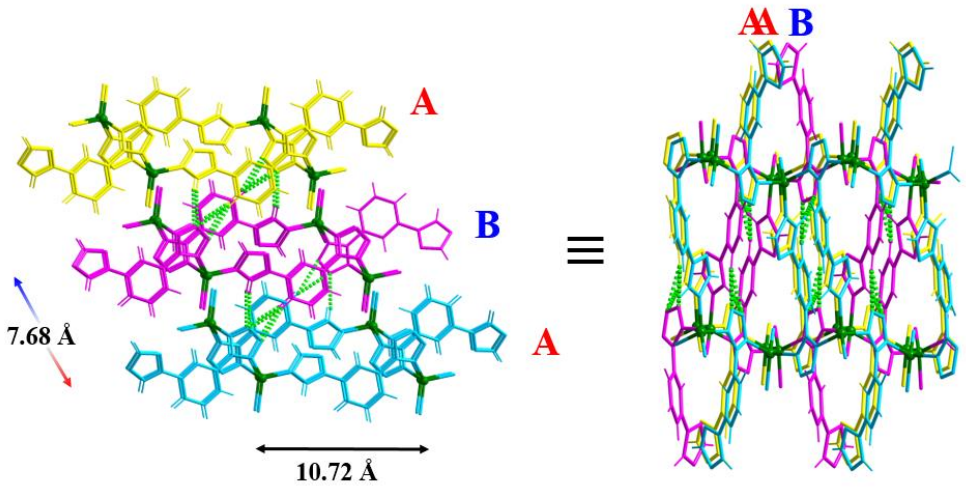

Figure S2. Packing diagram showing the interdigitating staggered arrangement of the 2D arrays (Each color represents one **fes** layer, Zn(II) centers are shown in green) and the hydrogen bonds as dashed lines in **1**.

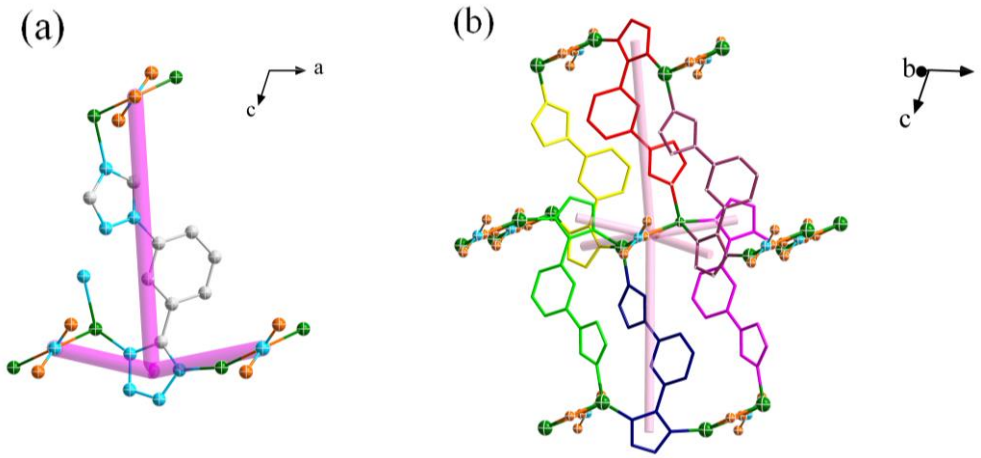

Figure S3. Representation of three-connected node of μ3-ttb^{-} (a) and 6-connected node of dizinc core (b) in **2**.

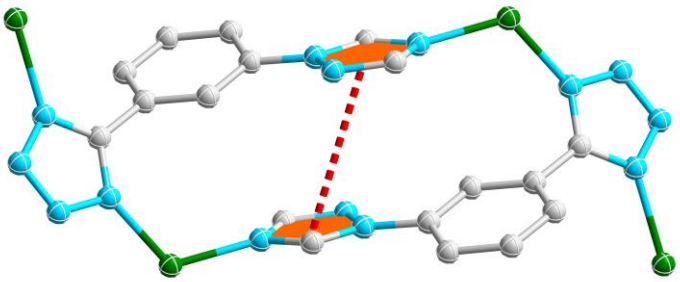

Figure S4. π···π interaction in **2**.

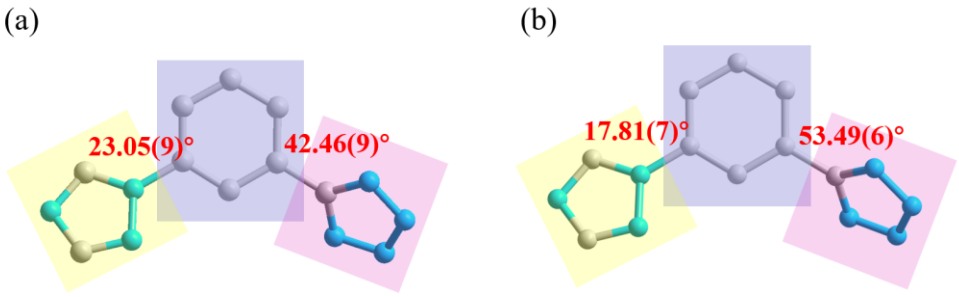

Figure S5. Schematic representation indicating the dihedral angles between the benzene ring and tetrazole/triazole rings, (a) for **1** and (b) for **2**.

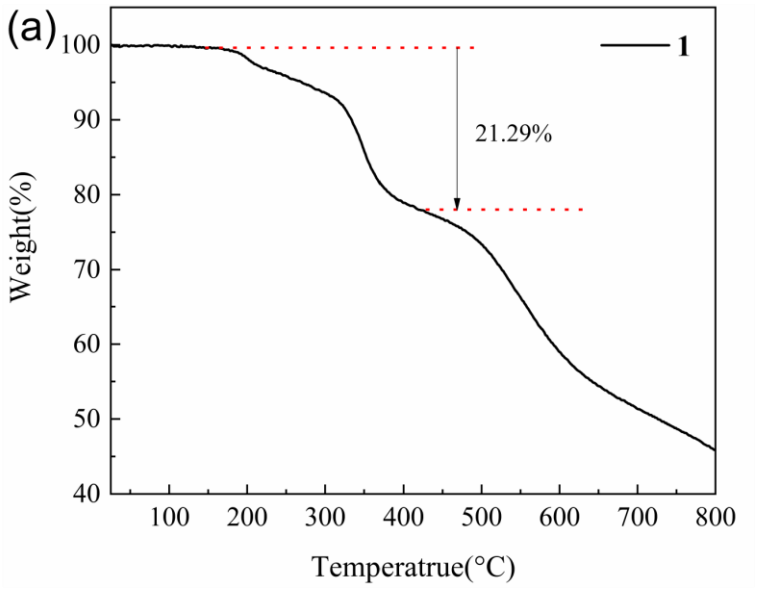

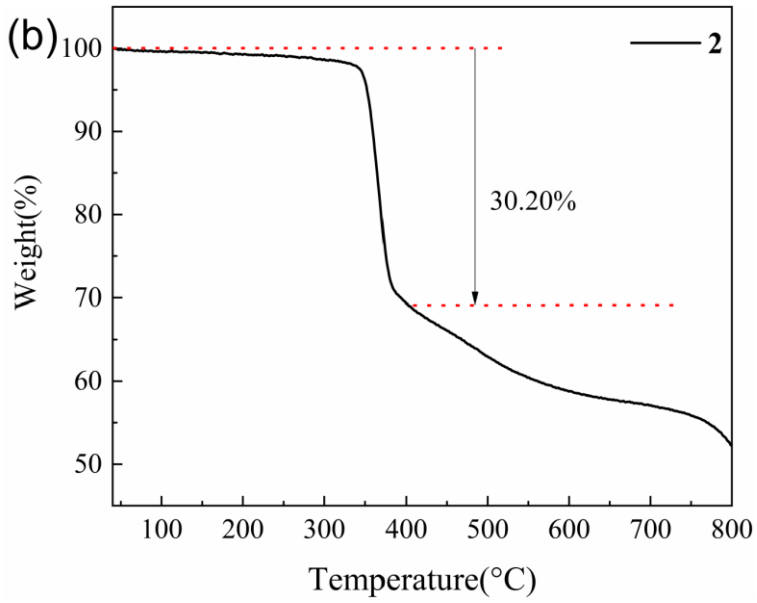

Figure S6. TGA curves of **1** (a) and **2** (b).

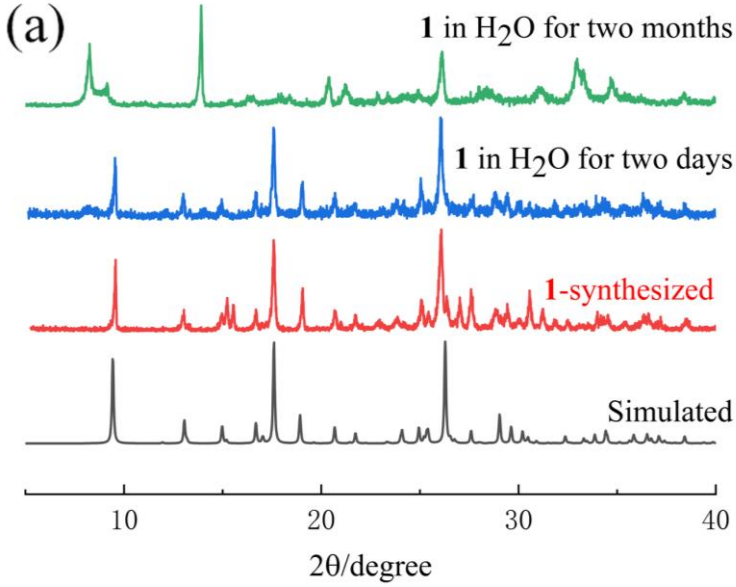

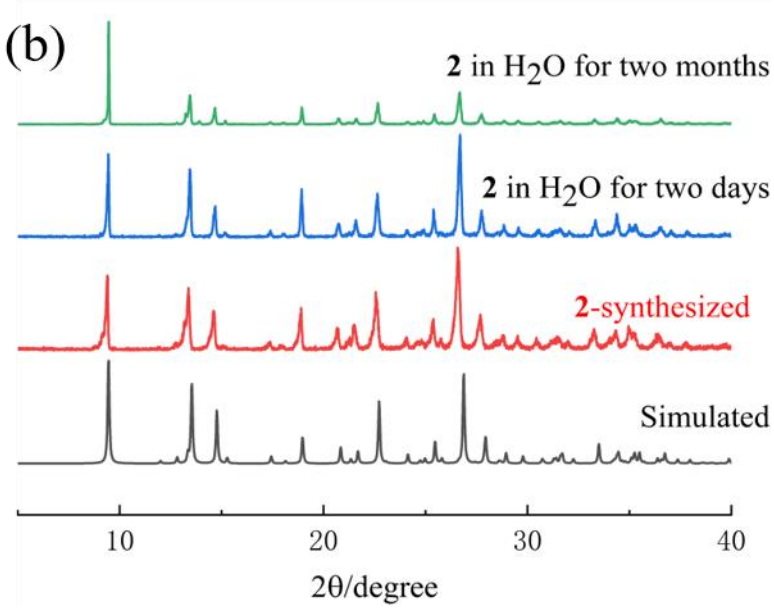

Figure S7. The PXRD patterns of **1** (a) and **2** (b).

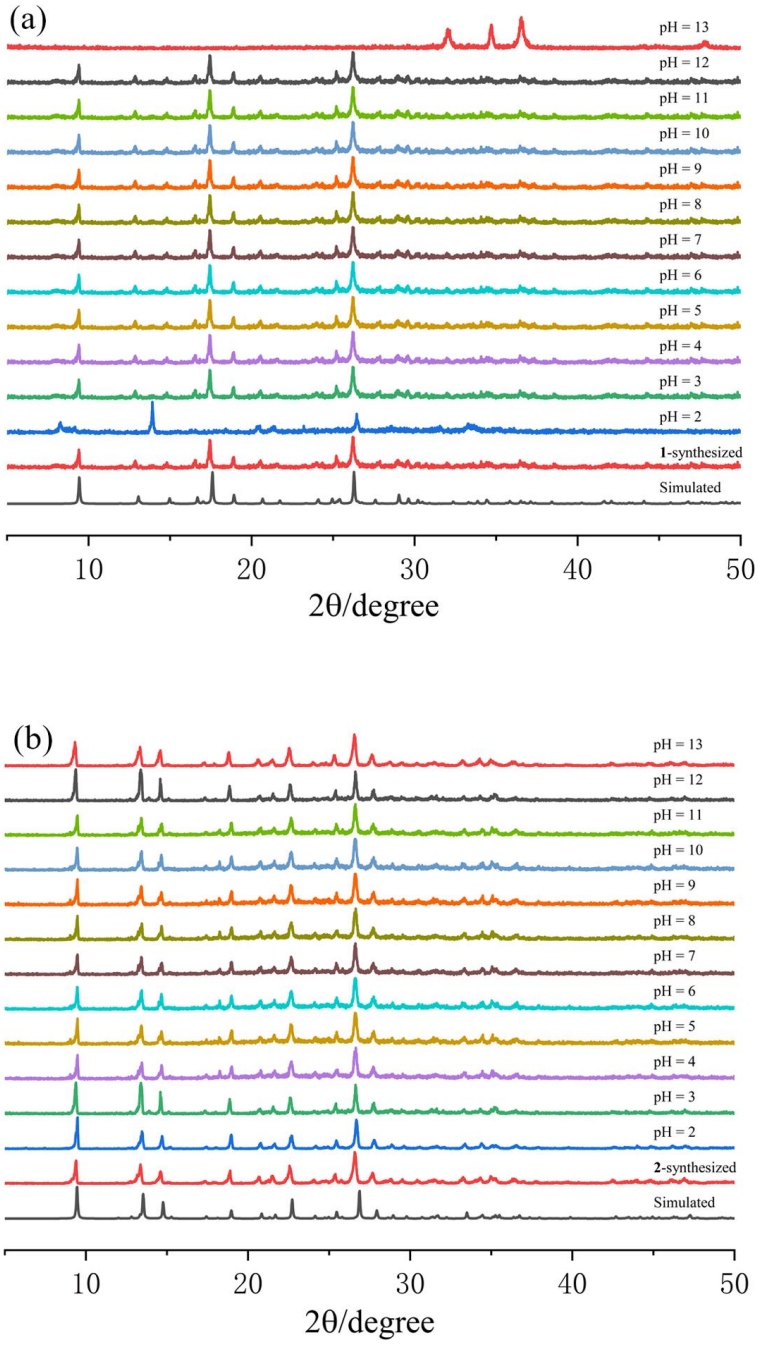

Figure S8. The PXRD patterns of **1** (a) and **2** (b) after being soaked in water, acidic, and basic solutions for 24 h using a wide pH range of 2.0~13.0.

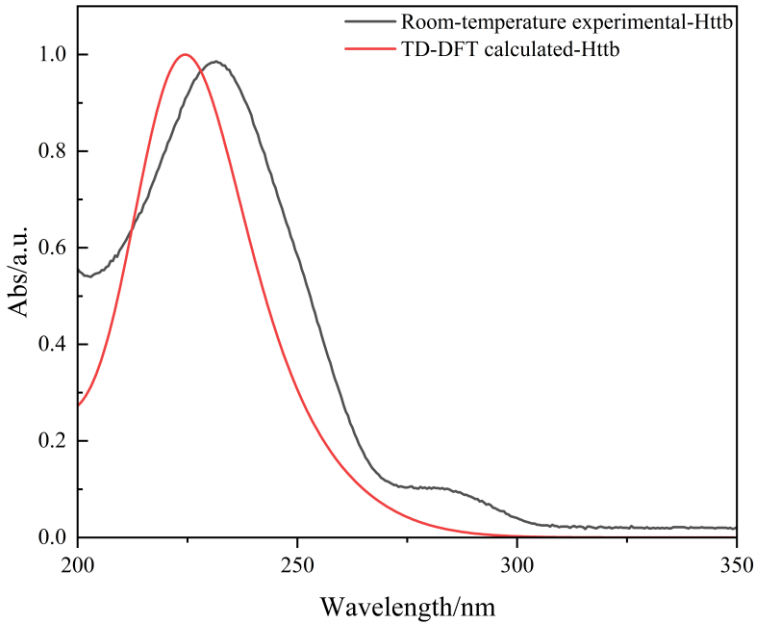

Figure S9. The UV absorption spectrum of the ligand (black) and by TD-DFT calculated (red).

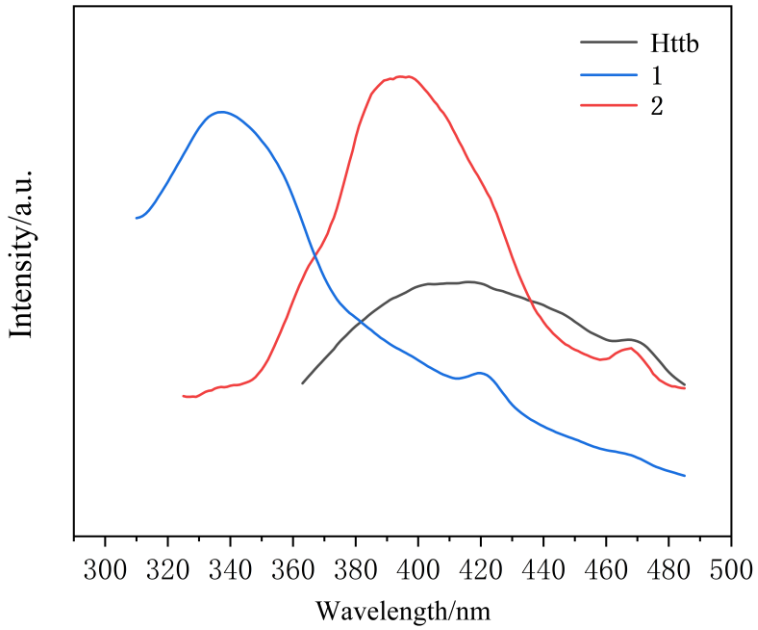

Figure S10. Solid-state fluorescence of **1**, **2** and Httb ligand.

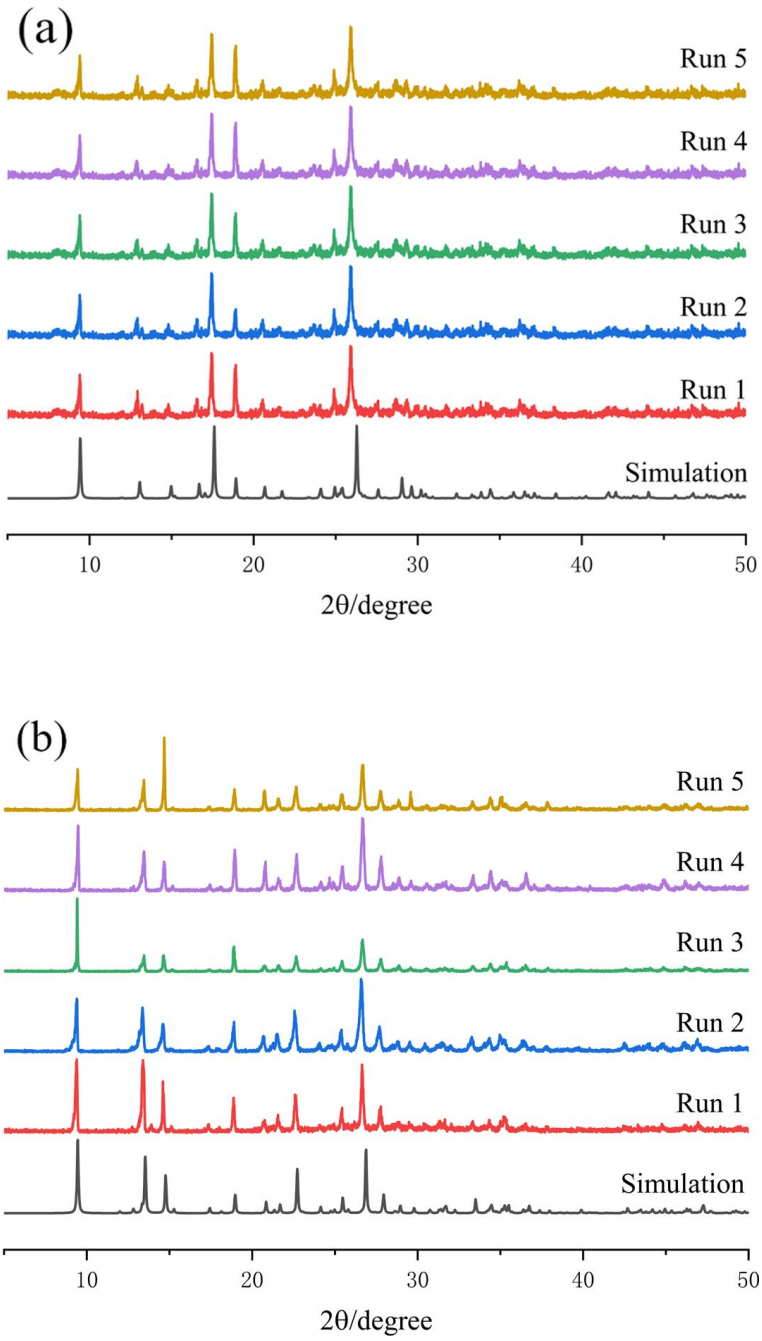

Figure S11. The PXRD pattern of **1** (a) and **2** (b) circulating five times in the tryptophan aqueous solution.

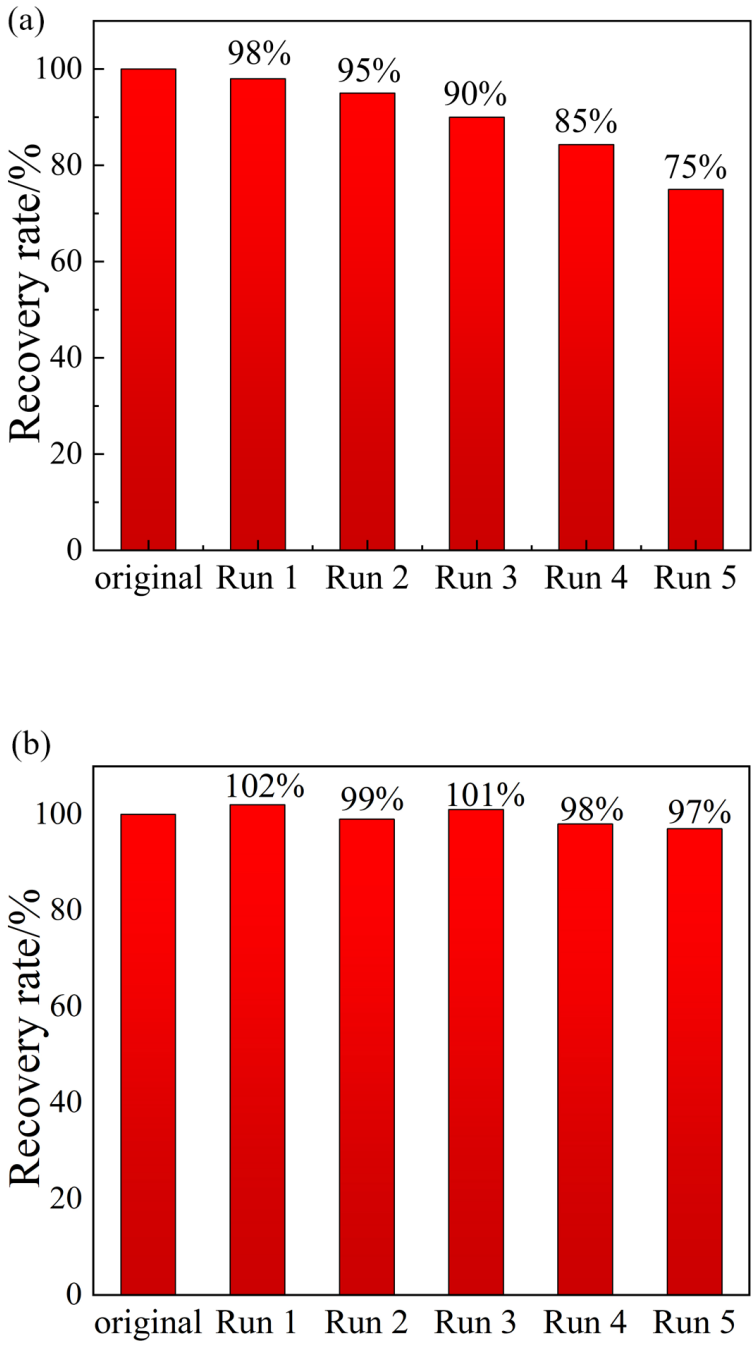

Figure S12. Recovery rate of **1** (a) and **2** (b) in cycle experiment.

The principle of MTS method to detect cell viability: MTS is a brand-new MTT analogue[1], the full name is 3-(4,5-dimethylthiazol-2-yl)-5(3-carboxymethoxyphenyl)-2-(4-sulfopheny)-2H-Tetrazolium is a yellow dye. Succinate dehydrogenase in the mitochondria of living cells can metabolize and reduce MTS to generate soluble formazan compounds. The content of formazan can be measured with a microplate reader at 490 nm. Normally The amount of formazan production is directly proportional to the number of living cells, so the number of living cells can be inferred from the OD value of the optical density.

Experimental method:

1. Cell inoculation: Use culture medium (DMEM) containing 10% fetal bovine serum to prepare a single cell suspension, inoculate 5000 cells per well into a 96-well plate, with a volume of 100 μl per well, and inoculate the cells 12-24 hours in advance. .

2. Add the test compound solution: the compound is dissolved in DMSO, and the compound is screened at the concentration of 20 μg/ml, 4 μg/ml, 0.8 μg/ml, 0.16 μg/ml, and the final volume of each well is 200 μl. Each treatment is set 3 multiple holes.

3. Color development: After culturing at 37 degrees Celsius for 48 hours, discard the culture medium in the cell, add 20 μl of MTS solution and 100μl of culture medium to each hole; set 3 blank multiple wells (a mixture of 20 μl of MTS solution and 100 μl of culture medium), and continue incubating Measure the light absorption value after allowing the reaction to proceed sufficiently for 2 to 4 hours.

4. Colorimetric: select the wavelength of 492 nm, read the light absorption value of each hole with a multifunctional microplate reader (MULTISKAN FC), record the

result, after data processing, draw the cell growth curve with the concentration as the abscissa and the cell survival rate as the ordinate, application The two-point method (Reed and Muench method) calculates the IC50 value of the compound.

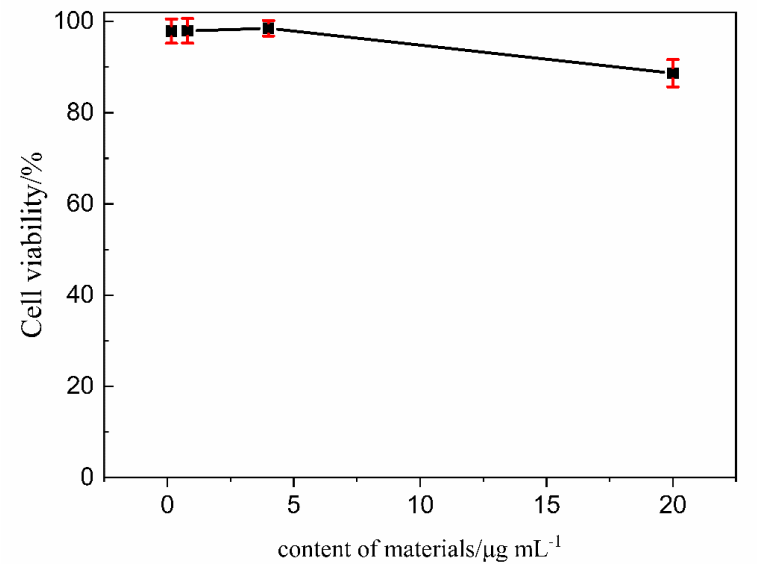

Figure S13. MTS assay of **2** obtained from incubation with BEAS-2B Cells.

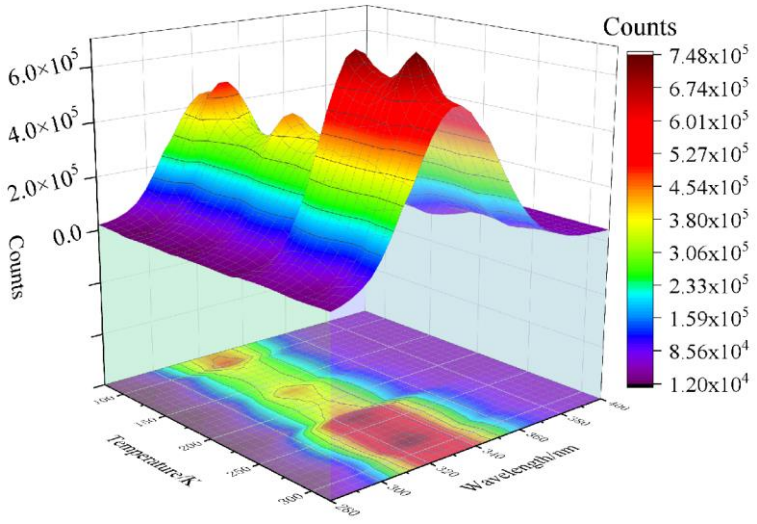

Figure S14. Variable temperature fluorescence of **2** (77K-317K).

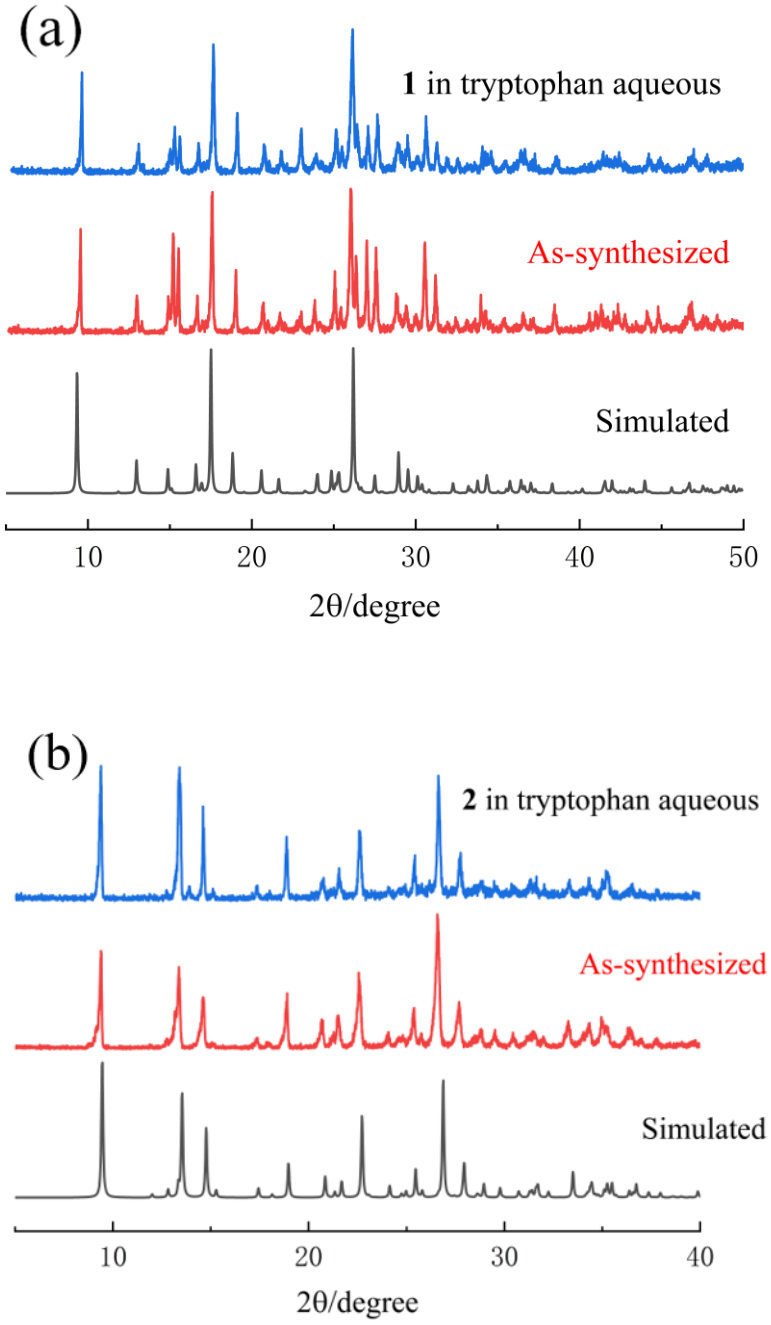

Figure S15. The PXRD pattern of **1** (a) and **2** (b) in tryptophan aqueous.

As shown in Figure S15, **1** and **2** did not collapse their skeletons after being immersed in the tryptophan aqueous solution. This shows that the quenching of the fluorescence by tryptophan is not caused by the collapse of the skeleton.

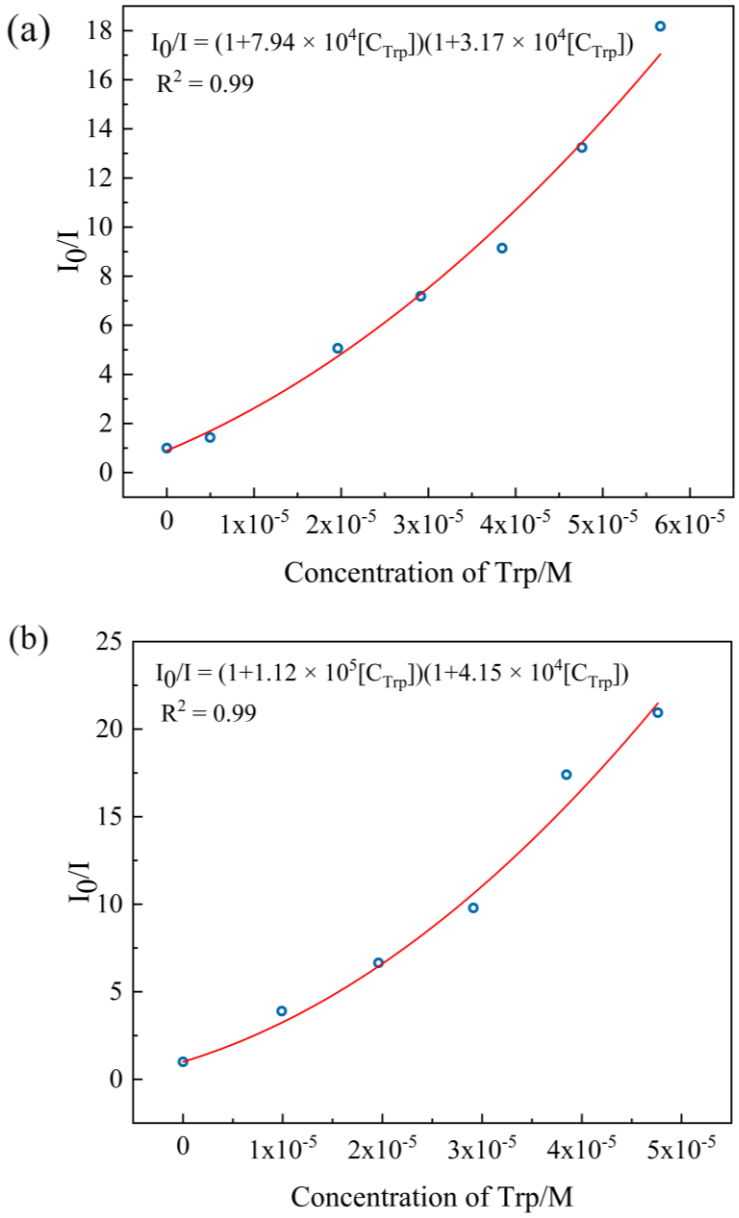

Figure S16. Nonlinear quenching plot of **1** (a) and **2** (b) with increasing tryptophan concentration.

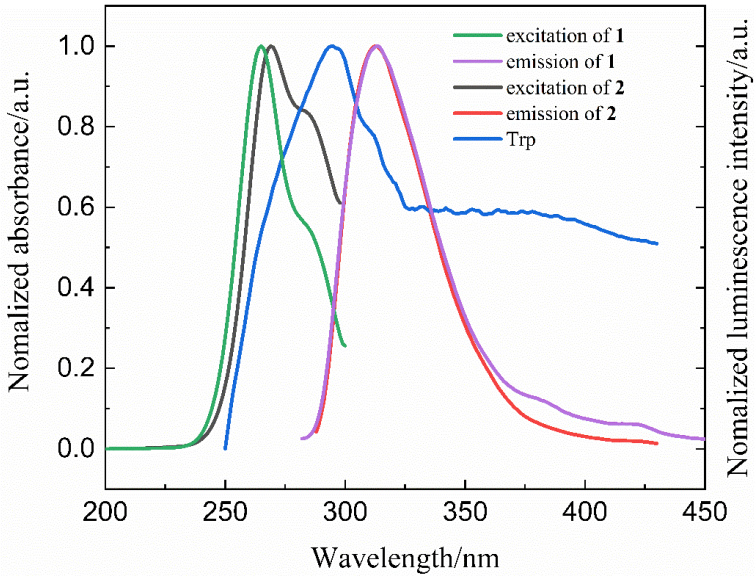

Figure S17. excitation wavelength and emission wavelength of **1** and **2** and tryptophan UV-Vis absorption spectrum.

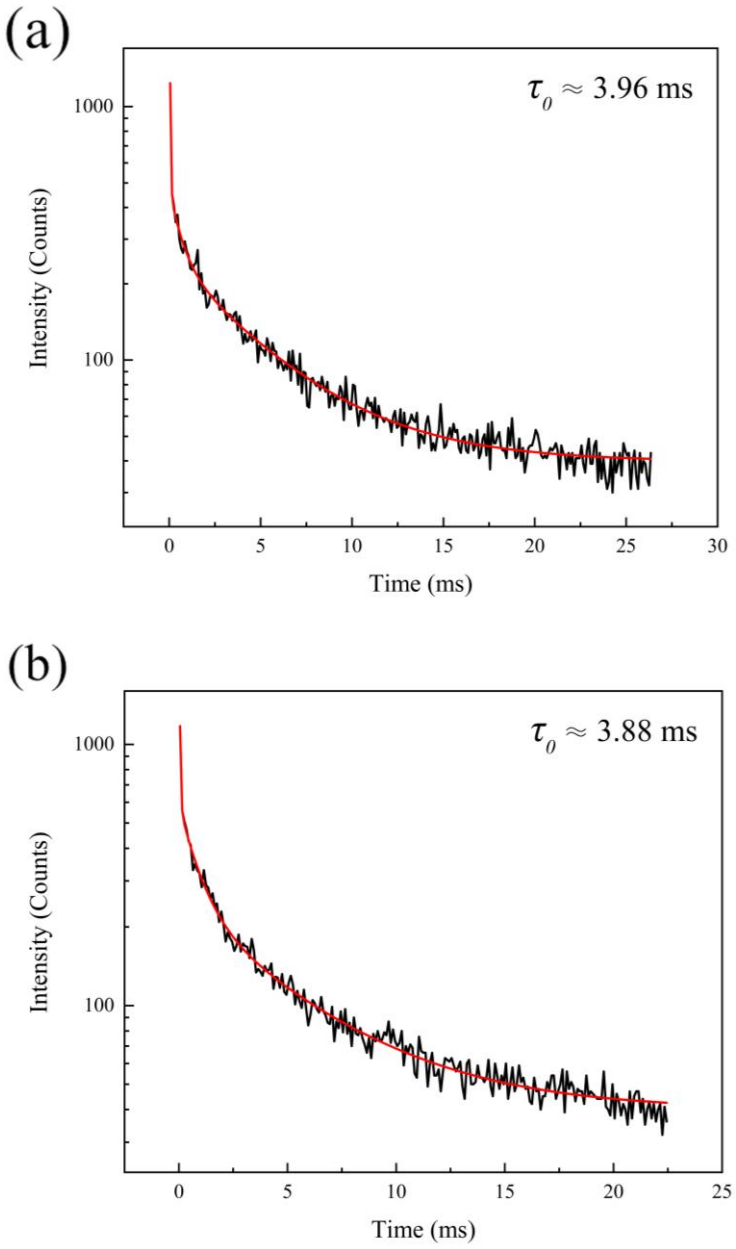

Figure S18. Fluorescence lifetime of **1** (a) and **2**(b).

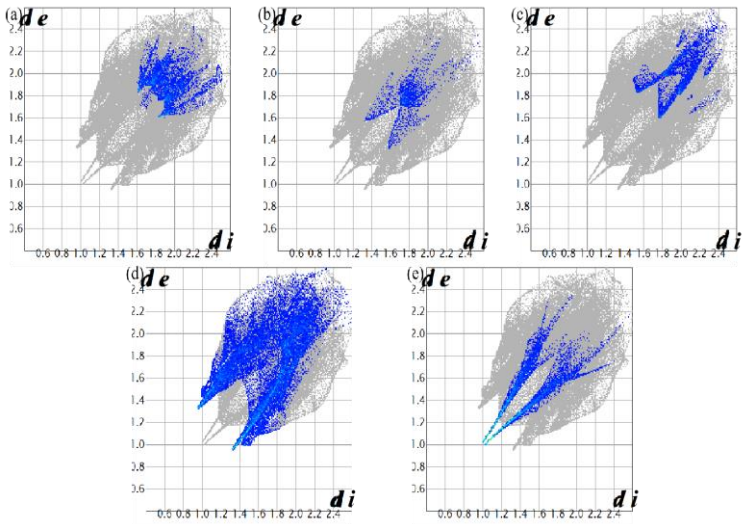

Figure S19. Two-dimensional fingerprint peak of **1** (Highlight close contacts from nitrogen to other elements and from other elements to nitrogen). (a)N···C surface area included 8.2%, (b)N···N surface area included 2.9%, (c)N···Cl surface area included 4.9%, (d)N···H surface area included 30.9%, (e)N…Zn surface area included 10.8%.

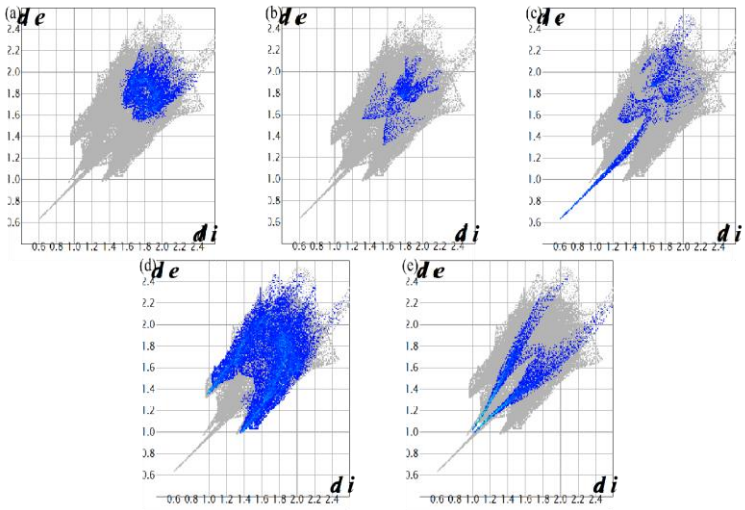

Figure S20. Two-dimensional fingerprint peak of **2** (Highlight close contacts from nitrogen to other elements and from other elements to nitrogen). (a)N···C surface area included 8.6%, (b)N···N surface area included 2.7%, (c)N···O surface area included 4.8%, (d)N···H surface area included 28.7%, (e)N···Zn surface area included 9.4%.

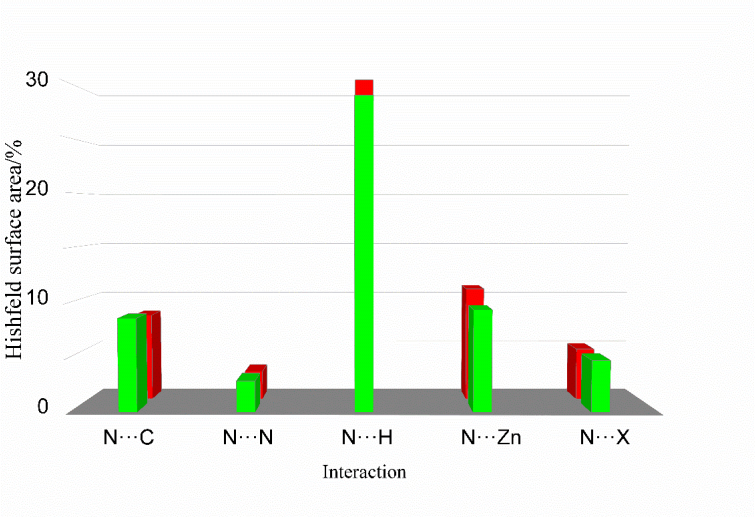

Figure S21. The relative contribution of the contacts between the various molecules and nitrogen atoms in **1** (red, X=Cl) and **2** (green, X=O) to Hirshfeld surface area.

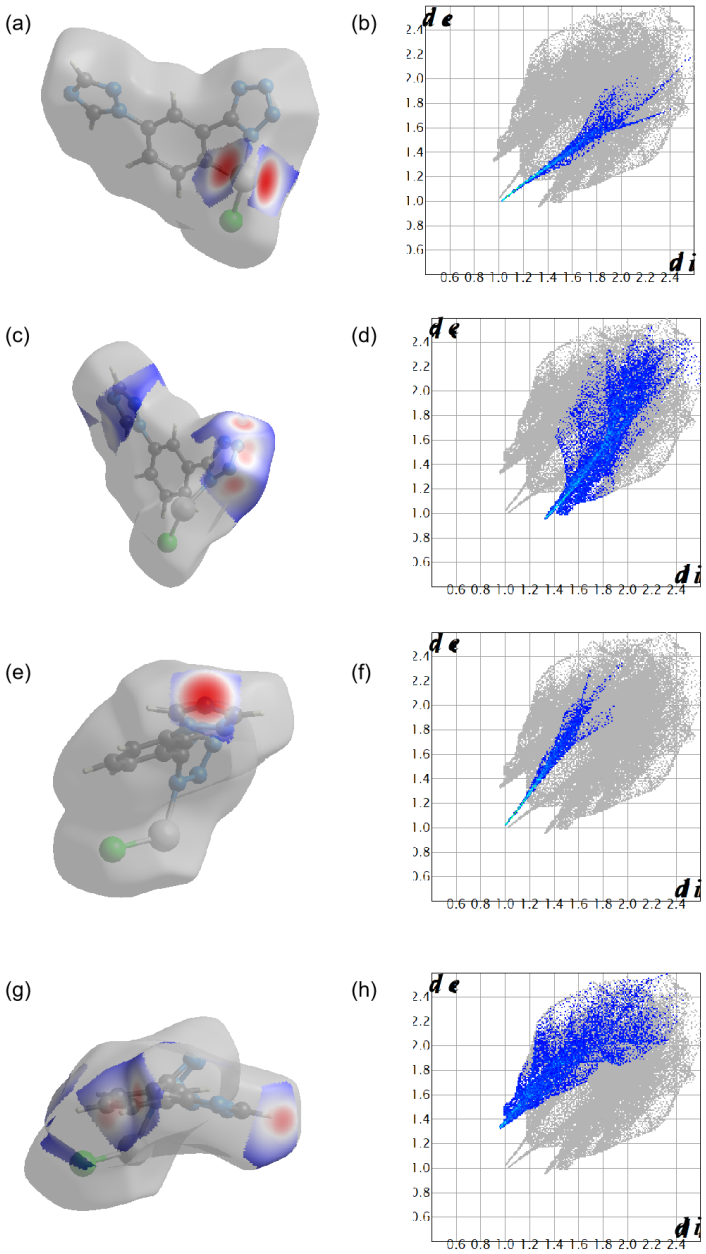

Figure S22. Hirshfeld surface mapped with d_{norm} of **1**. (a) The red area represented by a1, (b) 2D fingerprint peak corresponding to a1, (c) The red area represented by b1 and c1, (d) 2D fingerprint peaks corresponding to b1 and c1, (e) The red area represented by b2, (f) 2D fingerprint peak corresponding to b2, (g) The red area represented by b3 and c2, (h) 2D fingerprint peaks corresponding to b3 and c2.

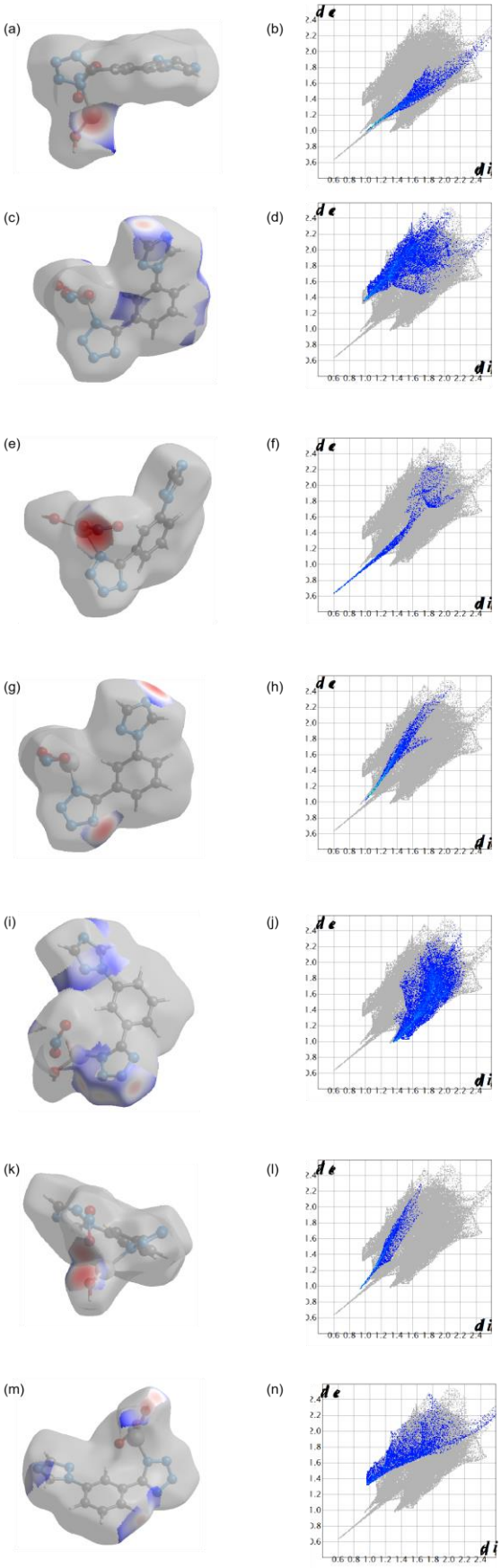
(a)
(b)
(c)
(d)
(e)
(f)
(g)
(h)
(i)
(j)
(k)
(l)
(m)
(n)

Figure S23. Hirshfeld surface mapped with d_{norm} of **2**. (a) The red area represented by a1, (b) 2D fingerprint peak corresponding to a1, (c) The red area represented by b1, (d) 2D fingerprint peak corresponding to b1, (e) The red area represented by b2, (f) 2D fingerprint peak corresponding to b2, (g) The red area represented by b3, (h) 2D fingerprint peak corresponding to b3, (i) The red area represented by b4, (j) 2D fingerprint peak corresponding to b4, (k) The red area represented by c1, (l) 2D fingerprint peak corresponding to c1, (m) the red area represented by c2, (n) 2D fingerprint peak corresponding to c2.

The distance of close contact interaction is analyzed by using the d_{norm} (normalized contact distance) function. In other words, it is the intermolecular interaction distance between the molecular sites of adjacent molecules and the molecular groups in the effective interaction area on the Hirshfeld surface.

$$d_{\text{norm}} = \frac{d_i - r_i^{VdW}}{r_i^{VdW}} + \frac{d_e - r_e^{VdW}}{r_e^{VdW}}$$

d_i and d_e are the distances from a point on the surface to the nearest nucleus outside and inside the Hirshfeld surface, respectively. r_i^{VdW} and r_e^{VdW} are the van der Waals radii of d_i and d_e atoms.[2, 3] The 2D fingerprint map drawn with d_i and d_e distances is a reduced 3D Hirshfeld surface format. The negative (red area) or positive (blue area) value of d_{norm} indicates that the intermolecular distance of the contact point is shorter or longer than the sum of r^{VdW}, respectively. Similarly, the zero (white area) value of d_{norm} means that the intermolecular distance of the contact point is equal to (or close to) the sum of r^{VdW}: therefore, the 3D d_{norm} Hirshfeld surface is mapped in red, blue, and white.[4,5]

Figure S22 shows the 3D Hirshfeld surface and 2D fingerprint peaks of each red area in **1**. It can be seen from Figures S20a and S20b that the formation of the red region is due to the N coordination of Zn(II) with another ligand. Figure S22c shows the red area of b1 and c1. The 2D fingerprint peak can be seen as the interaction of N···H, and c1 is also due to the interaction of N···H (Figure S22d). Figure S22e shows the red area of b2. According to the 2D fingerprint peak analysis, the red area is the interaction between N and Zn(II) (Figure S22f). Then, b3 and c2 are the interactions of H···N (Figure S22g-S22h).

Figure S23 shows the 3D Hirshfeld surface and 2D fingerprint peaks of each red area in **2**. It can be seen from Figures S23a and S23b that the formation of the red region is due to the N coordination between Zn(II) and another ligand. Figure S23c shows the red area of b1, and the 2D fingerprint peak can be seen as the interaction of H···N (Figure S23d). Figure S23e shows the red area of b2. According to the 2D fingerprint peak analysis, the red area is the interaction of N in nitrate with another O that is not shown (Figure S23f). Then, b3 is the coordination effect of N and other Zn(II) (Figure S23g-S23h). Figure S23i shows the red area of b4, which is found to be the interaction between N···H according to the 2D fingerprint peaks (Figure S23j). c1 represents the interaction between the oxygen atom in the hydroxide radical and the other Zn(II) bridged. (Figure S23k-S23l). Figure S23m shows the red area of c2, which is due to the interaction between H···O. Based on these, we found that in **1** and **2**, in addition to the coordination bond, the main reason is the hydrogen bond. This can also be shown more intuitively through Figure 8 and S23.

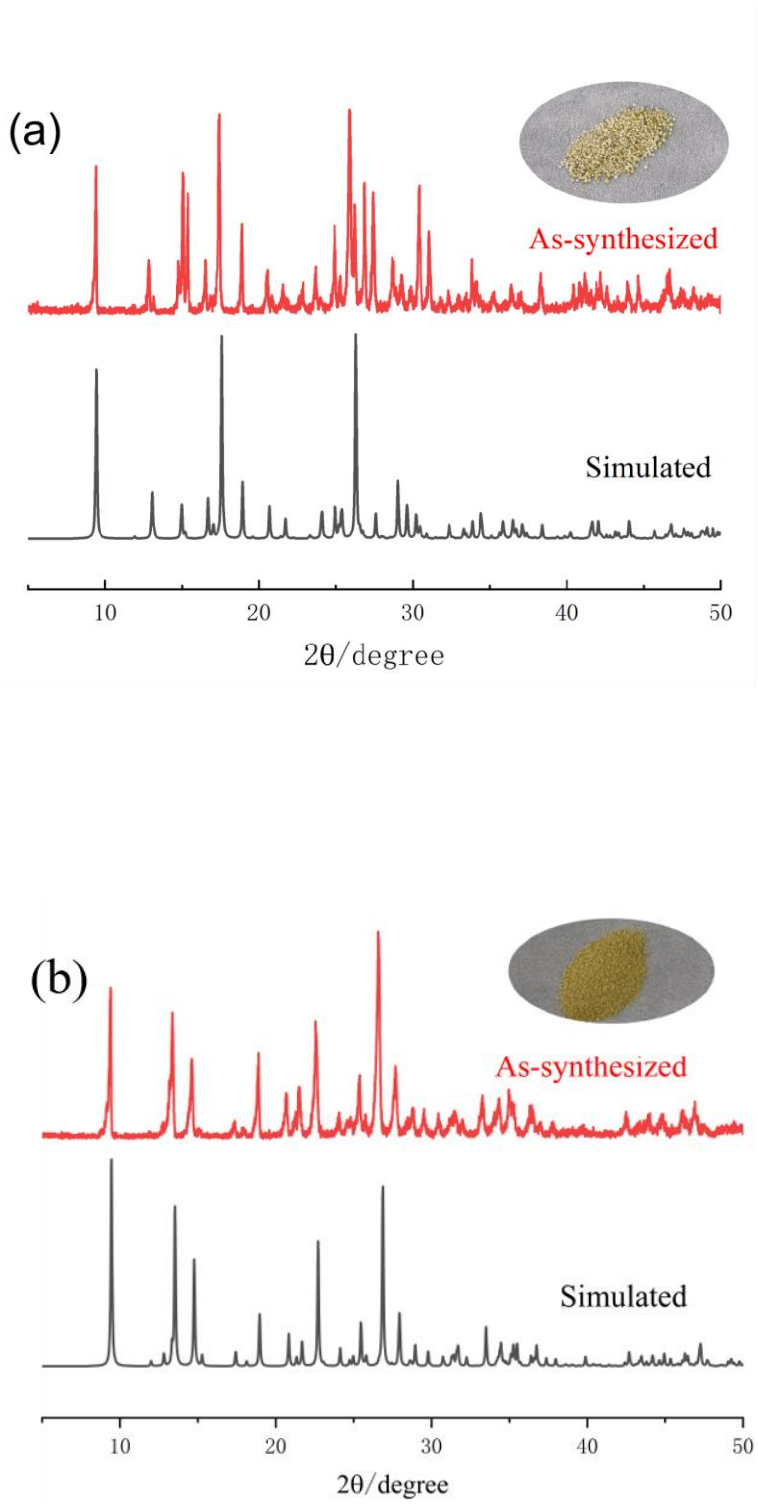

Figure S24. The PXRD patterns of **1** (a) and **2** (b), the upper right corner of each picture is the actual powder picture.

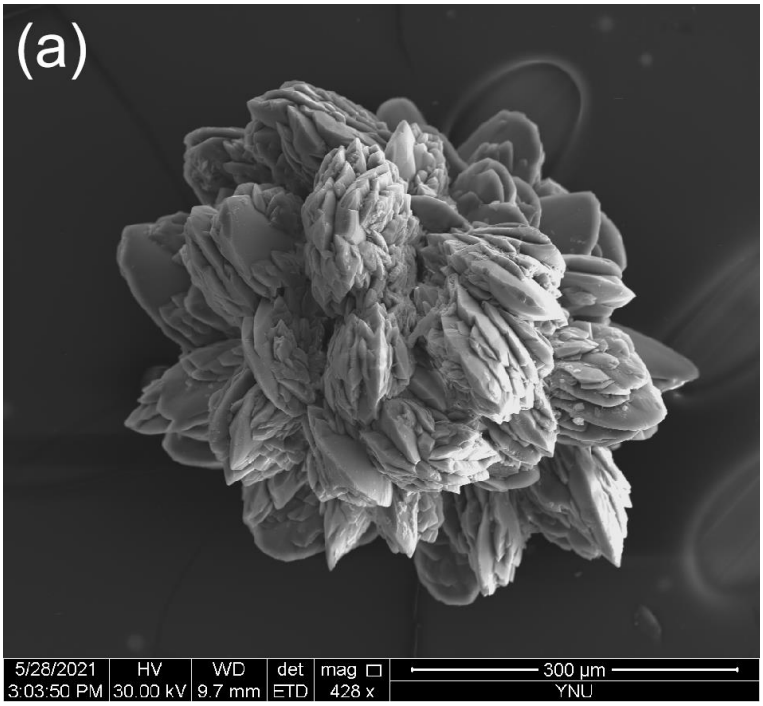

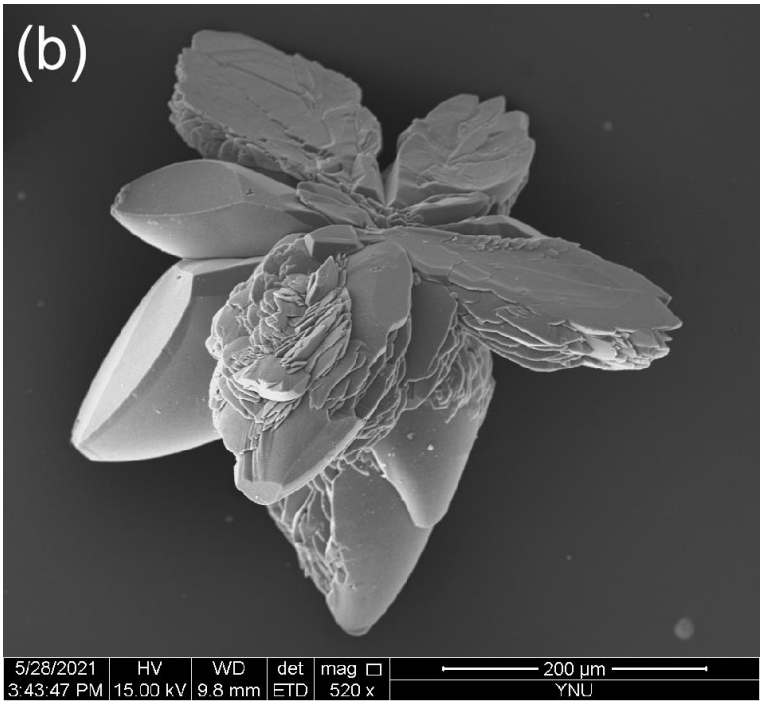

Figure S25. SEM of **1** (a) and **2** (b).

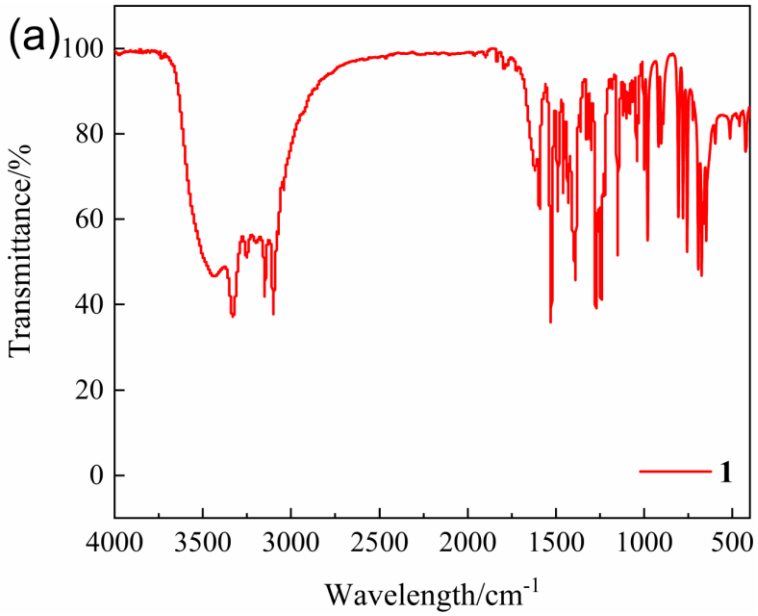
(a)
100
80
60
40
20
0
Transmittance/%
1
4000
3500
3000
2500
2000
1500
1000
500
Wavelength/cm-1

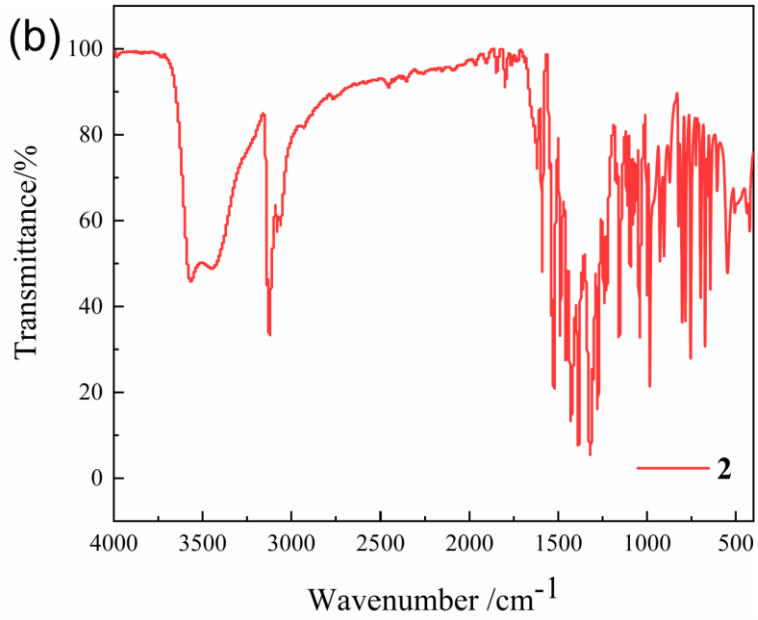
(b)
100
80
60
40
20
0
Transmittance/%
2
4000
3500
3000
2500
2000
1500
1000
500
Wavenumber /cm-1

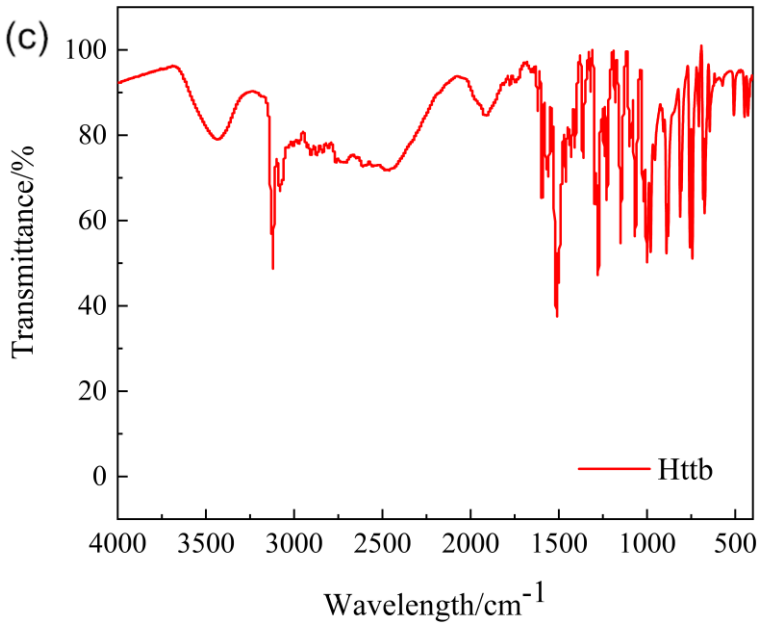

Figure S26. The Infrared Spectroscopy of **1** (a), **2** (b), and Httb (c).

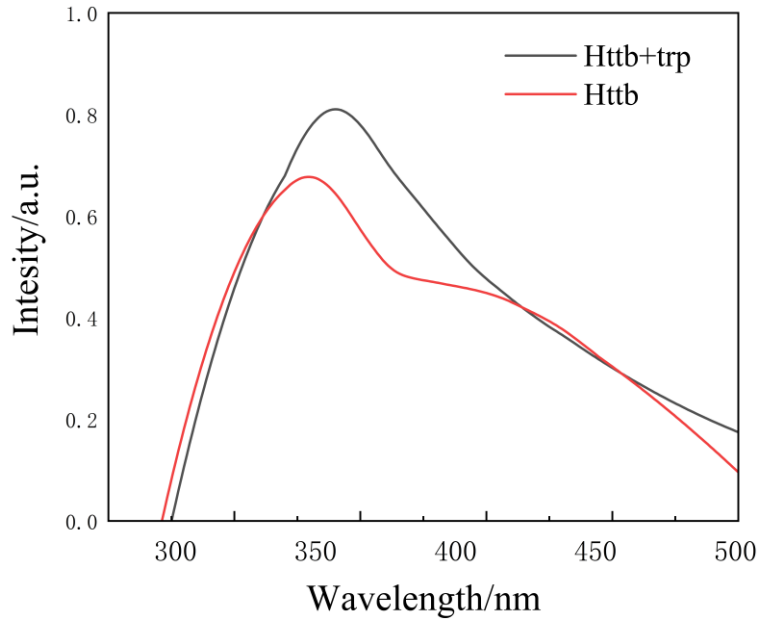

Figure S27. Liquid Fluorescence of Ligand (red line) and the fluorescence curve after adding tryptophan (black line).

According to Figure S27, the ligand cannot detect tryptophan.

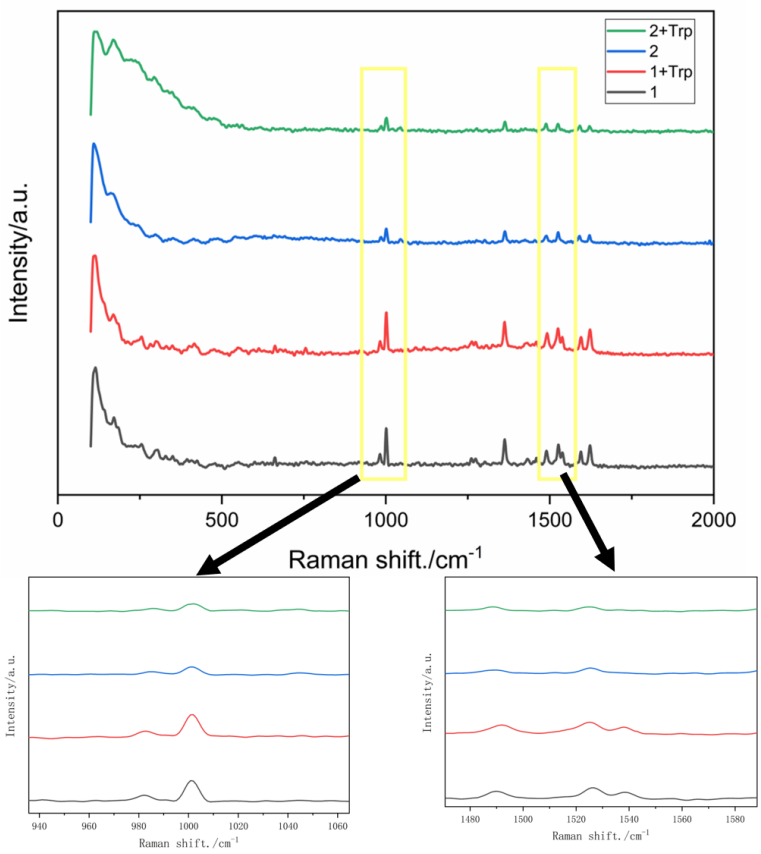

Figure S28. Raman spectra of **1**, **2** and after adding tryptophan respectively.

Table S1. Crystallographic data for **1** and **2**.

Httb	**1**	**2**
CCDC no.	2051367	2052792
empirical formula	$C_9H_6ClN_7Zn$	$C_9H_{6.5}N_{7.5}O_2Zn$
formula weight	313.03	317.09
crystal system	Monoclinic	Monoclinic
space group	$P2_1/c$	$C2/c$
a (Å)	9.6998(4)	15.4732(4)
b (Å)	7.6212(4)	7.4234(2
c (Å)	15.3208(6)	19.6348(5)
α (°)	90	90
β (°)	104.921(2)	107.7590(10)
γ (°)	90	90
V (Å^3)	1094.39(9)	2147.86(10)
Z	4	8
ρ calc (mg m^{-3})	1.9	1.961
μ (mm^{-1})	2.479	2.302
F(000)	624	1272
Crystal size (mm^3)	0.00792	0.01056
Reflections collected	7421	10225
independent reflections	1949	1909
GOF	1.036	1.074
R_1, wR_2 [I> 2σ(I)][b]	0.0283, 0.0556	0.0232,0.0536
R_1, wR_2 (all data)[b]	0.0408, 0.0613	0.028, 0.0564
$\Delta\rho_{max}$, $\Delta\rho_{min}$ (e Å^{-3})	0.353, –0.328	0.269, –0.298

Table S2. Selected bond distances and angles for **1**

bond distance	(Å)	bond distance	(Å)
Zn1—N1^{i}	2.027 (2)	N4—Zn1^{iv}	2.032 (2)
Zn1—N4^{ii}	2.032 (2)	N1—Zn1^{iii}	2.027 (2)
Zn1—N7	2.062 (2)	Zn1—Cl1	2.2002 (8)
angle	(°)	angle	(°)
N1^{i}—Zn1—N4^{ii}	118.36 (9)	N5—N4—Zn1^{iv}	117.34 (17)
N1^{i}—Zn1—N7	103.43 (9)	C9—N7—Zn1	130.10 (19)
N4^{ii}—Zn1—N7	90.13 (9)	N6—N7—Zn1	119.74 (18)
N1^{i}—Zn1—Cl1	109.11 (7)	C2—N1—Zn1^{iii}	127.68 (19)
N4^{ii}—Zn1—Cl1	113.70 (7)	C1—N1—Zn1^{iii}	127.76 (19)
N7—Zn1—Cl1	121.25 (7)	C9—N4—Zn1^{iv}	133.46 (19)

Symmetry codes: (i) $x + 1, 1/2 - y, z + 1/2$; (ii) $1 - x, y+1/2, 3/2 - z$; (iii) $x - 1, 1/2 - y, z - 1/2$; (iv) $1 - x, y - 1/2, 3/2 - z$.

Table S3. Selected bond distances and angles for **2**

bond distance	(Å)	bond distance	(Å)
N1—Zn1^{i}	2.0246 (18)	O3—Zn1	1.9127 (9)
N4—Zn1	2.0409 (16)	O3—Zn1^{iii}	1.9127 (9)
N7—Zn1^{ii}	2.1048 (17)	Zn1—N7^{iv}	2.1048 (17)
O1—Zn1^{iii}	2.3493 (13)	O1—Zn1	2.3493 (13)
angle	(°)	angle	(°)
C1—N1—Zn1^{i}	128.71 (15)	O3—Zn1—N4	128.97 (5)
C2—N1—Zn1^{i}	127.44 (15)	O3—Zn1—N7^{iv}	106.87 (7)
N5—N4—Zn1	122.23 (13)	O3—Zn1—O1	72.46 (6)
C9—N4—Zn1	129.38 (14)	N8—O1—Zn1^{iii}	134.19 (3)
N6—N7—Zn1^{ii}	123.99 (13)	N8—O1—Zn1	134.19 (3)
C9—N7—Zn1^{ii}	126.62 (14)	Zn1^{iii}—O1—Zn1	91.63 (7)
N1^{i}—Zn1—O1	93.05 (5)	Zn1—O3—Zn1^{iii}	123.46 (10)
N4—Zn1—N7^{iv}	88.39 (7)	Zn1—O3—H3	118.27 (5)
N4—Zn1—O1	80.29 (5)	Zn1^{iii}—O3—H3	118.27 (5)
N7^{iv}—Zn1—O1	163.83 (5)	N1^{i}—Zn1—N4	119.11 (7)
O3—Zn1—N1^{i}	104.89 (5)	N1^{i}—Zn1—N7^{iv}	102.58 (7)

Symmetry codes: (i) 1 − *x*, 1 − *y*, 1 − *z*; (ii) 3/2 − *x*, *y* + 1/2, 3/2 − *z*; (iii) 1 − *x*, *y*, 3/2 − *z*; (iv) 3/2 − *x*, *y* − 1/2, 3/2 − *z*.

Table S4. Hydrogen bonds for **1**

D–H···A	D–H (Å)	H···A (Å)	D···A (Å)	D···H···A (°)
C1–H1···N6(A)	0.95	2.37	3.097(4)	133
C2–H2···N5(B)	0.95	2.40	3.312(4)	160
C8–H8···N5(B)	0.95	2.60	3.502(4)	159
C8–H8···N6(B)	0.95	2.56	3.475(4)	162

Symmetry codes: (A) *x* – 1, –*y* + 1/2, *z* – 1/2; (B) *x* – 1, *y*, *z*.

Table S5. Hydrogen bonds for **2**

D–H···A	D–H (Å)	H···A (Å)	D···A (Å)	D···H···A (°)
C1–H1···N6(A)	0.93	2.45	3.175(3)	135
C2–H2A···N5(B)	0.93	2.50	3.322(3)	148
C4–H4···N2	0.93	2.51	3.824(3)	100
C6–H6···O2(C)	0.93	2.55	3.391(3)	151
O3–H3···O2(D)	0.81	2.45	3.195(3)	154
O3–H3···O2(E)	0.81	2.45	3.195(3)	154

Symmetry codes: (A) $x - 1/2, 3/2 - y, z - 1/2$; (B) $x, 1 - y, z - 1/2$; (C) $1/2 + x, y - 1/2, z$; (D) $x, y - 1, z$;(E) $1 - x, y - 1, 3/2 - z$.

Table S6. Calculate the S1 electron transfer energy of the ligand and the contribution rate of each orbital.

	UV = 223.08 nm	f = 0.9820
MOs		the contribution rate
HOMO-1	→ LUMO	28.2%
HOMO-1	→ LUMO+1	5.7%
HOMO	→ LUMO+1	58.2%

Table S7. Calculation results of singlet state energy level and the corresponding wavelength of excitation light of Httb and selected amino acids.

Amino acids	Singlet state energy level (eV)	Excitation light wavelength (nm)
Alanine	5.2382	236.69
Arginine	5.2456	236.36
Asparagine	5.1484	240.82
Aspartic Acid	5.2749	235.04
Cysteine	5.1767	239.5
Glutamine	5.3442	232
Glutamic Acid	5.3536	231.59
Glycine	5.4098	229.19
Histidine	4.6439	266.98
Isoleucine	5.3979	229.69
Leucine	5.2784	234.89
Lysine	5.4104	229.16
Methionine	5.3779	230.54
Phenylalanine	4.9072	252.66
Proline	5.1332	241.54
Serine	5.2474	236.28
Threonine	5.2171	237.65
Tryptophan	**4.3051**	**287.99**
Tyrosine	4.878	254.17
Valine	5.3902	230.02
Httb	**4.2089**	**294.58**

The calculation of the ligand was performed using the Gaussian 09 program.[6] The calculation of amino acids comes from the report of Qian's group.[7] The structure was completely optimized to the ground state by the DFT method at B3LYP/6-311+g(d,p) level. Then the singlet and triplet energy of structures were calculated based on TD-SCF method.

REFERENCES

1. Gencoglu, M. F.; Spurri, A.; Franko, M.; Chen, J.; Hensley, D. K.; Heldt, C. L.; Saha, D., Biocompatibility of soft-templated mesoporous carbons. *ACS Applied Materials & Interfaces* **2014**, *6* (17), 15068-77.

2. Parwani, A. V., Expression of Glypican 3 in Ovarian and Extragonadal Germ Cell Tumors. *Yearbook of Pathology and Laboratory Medicine* **2009**, *2009*, 93-95.

3. Momeni, B. Z.; Rahimi, F.; Torrei, M.; Rominger, F., Synthesis, Hirshfeld surface analysis, luminescence and thermal properties of three first-row transition metal complexes containing 4′-hydroxy-2,2′:6′,2″-terpyridine: Application for preparation of nano metal oxides. *Applied Organometallic Chemistry* **2020**, *34* (5).

4. M.A. Spackmann, J.J. McKinnon, D. Jayatilaka., Electrostatic potentials mapped on Hirshfeld surfaces provide direct insight into intermolecular interactions in crystals *CrystEngComm* **2008**, *10*, 377.

5. Gökce, H.; Alpaslan, G.; Alaşalvar, C., Crystal structure, spectroscopic characterization, DFT computations and molecular docking study of a synthesized Zn(II) complex. *Journal of Coordination Chemistry* **2019**, *72* (5-7), 1075-1096.

6. Gaussian 09, Revision D.01, M. J. Frisch, G. W. Trucks, H. B. Schlegel, G. E. Scuseria, M. A. Robb, J. R. Cheeseman, G. Scalmani, V. Barone, B. Mennucci, G. A. Petersson, H. Nakatsuji, M. Caricato, X. Li, H. P. Hratchian, A. F. Izmaylov, J. Bloino, G. Zheng, J. L. Sonnenberg, M. Hada, M. Ehara, K. Toyota, R. Fukuda, J. Hasegawa,

M. Ishida, T. Nakajima, Y. Honda, O. Kitao, H. Nakai, T. Vreven, J. A. Montgomery, Jr., J. E. Peralta, F. Ogliaro, M. Bearpark, J. J. Heyd, E. Brothers, K. N. Kudin, V. N. Staroverov, T. Keith, R. Kobayashi, J. Normand, K. Raghavachari, A. Rendell, J. C. Burant, S. S. Iyengar, J. Tomasi, M. Cossi, N. Rega, J. M. Millam, M. Klene, J. E. Knox, J. B. Cross, V. Bakken, C. Adamo, J. Jaramillo, R. Gomperts, R. E. Stratmann, O. Yazyev, A. J. Austin, R. Cammi, C. Pomelli, J. W. Ochterski, R. L. Martin, K. Morokuma, V. G. Zakrzewski, G. A. Voth, P. Salvador, J. J. Dannenberg, S. Dapprich, A. D. Daniels, O. Farkas, J. B. Foresman, J. V. Ortiz, J. Cioslowski, and D. J. Fox, Gaussian, Inc., Wallingford CT, **2013**.

7. Zhang, J.; Huang, Y.; Yue, D.; Cui, Y.; Yang, Y.; Qian, G., A luminescent turn-up metal-organic framework sensor for tryptophan based on singlet-singlet Forster energy transfer. *Journal of Materials Chemistry B* **2018**, *6* (31), 5174-5180.